Matilde Barón*, Mónica Pineda and María Luisa Pérez-Bueno

Picturing pathogen infection in plants

DOI 10.1515/znc-2016-0134
Received June 30, 2016; revised July 21, 2016; accepted July 22, 2016

Abstract: Several imaging techniques have provided valuable tools to evaluate the impact of biotic stress on host plants. The use of these techniques enables the study of plant-pathogen interactions by analysing the spatial and temporal heterogeneity of foliar metabolism during pathogenesis. In this work we review the use of imaging techniques based on chlorophyll fluorescence, multicolour fluorescence and thermography for the study of virus, bacteria and fungi-infected plants. These studies have revealed the impact of pathogen challenge on photosynthetic performance, secondary metabolism, as well as leaf transpiration as a promising tool for field and greenhouse management of diseases. Images of standard chlorophyll fluorescence (Chl-F) parameters obtained during Chl-F induction kinetics related to photochemical processes and those involved in energy dissipation, could be good stress indicators to monitor pathogenesis. Changes on UV-induced blue (F440) and green fluorescence (F520) measured by multicolour fluorescence imaging in pathogen-challenged plants seem to be related with the up-regulation of the plant secondary metabolism and with an increase in phenolic compounds involved in plant defence, such as scopoletin, chlorogenic or ferulic acids. Thermal imaging visualizes the leaf transpiration map during pathogenesis and emphasizes the key role of stomata on innate plant immunity. Using several imaging techniques in parallel could allow obtaining disease signatures for a specific pathogen. These techniques have also turned out to be very useful for presymptomatic pathogen detection, and powerful non-destructive tools for precision agriculture. Their applicability at lab-scale, in the field by remote sensing, and in high-throughput plant phenotyping, makes them particularly useful. Thermal sensors are widely used in crop fields to detect early changes in leaf transpiration induced by both air-borne and soil-borne pathogens. The limitations of measuring photosynthesis by Chl-F at the canopy level are being solved, while the use of multispectral fluorescence imaging is very challenging due to the type of light excitation that is used.

Keywords: biotic stress; chlorophyll fluorescence imaging; multicolor fluorescence imaging; plant pathogens; thermography.

Abbreviations: BGF, blue-green fluorescence; Chl-F, chlorophyll fluorescence; Chl-FI, chlorophyll fluorescence imaging; F440, blue fluorescence; F520, green fluorescence; F680, red fluorescence; F740, far red fluorescence; F_{PSII}, effective quantum yield of photosystem II; F_V/F_M, maximum quantum efficiency of photosystem II; GLRaV-3, *Grapevine leafroll associated virus 3*; HD, high dose; HR, hypersensitive response; LD, low dose; MCFI, multicolour fluorescence imaging; NIR, near infrared; ObPV, *Obuda pepper virus*; PAMPs, pathogen-associated molecular patterns; PMMoV, *Pepper mild mottle virus*; Pph, *Pseudomonas syringae* pv. *phaseolicola*; Psa, *Pseudomonas syringae* pv. *actinidiae*; PSII, photosystem II; Pto, *Pseudomonas syringae* pv. tomato; PVY, *Potato virus Y*; RFd, red chlorophyll fluorescence decrease ratio; TMV, *Tobacco mosaic virus*.

Dedication: This work is dedicated to the memory of Professor Peter Böger. He will always bring to my heart (M. B.) the best memories of my postdoc at Lake Constance.

1 Imaging techniques for biotic stress detection

Plant diseases induced by pathogens such as viruses, bacteria and fungi are responsible for major economic losses in agriculture worldwide. Early detection of pathogens is essential to reduce disease spread and facilitate plant protection practices.

Non-invasive techniques to image the patterns of multispectral fluorescence or leaf temperature across infected leaves have greatly increased our understanding of plant responses to biotic stress [1, 2]. Visualization of the light signals emitted by plants can track the spreading of a pathogen through its host [3–5]. Furthermore, these techniques could be very useful for presymptomatic stress detection, depending on the extent in the changes

***Corresponding author: Matilde Barón,** Department of Biochemistry, Molecular and Cell Biology of Plants, Estación Experimental del Zaidín, Spanish Council of Scientific Research (CSIC), Profesor Albareda 1, 18008 Granada, Spain,
Phone: +34 958 18 16 00 Ext. 213, Fax: +34 958 12 96 00,
E-mail: mbaron@eez.csic.es
Mónica Pineda and María Luisa Pérez-Bueno: Department of Biochemistry, Molecular and Cell Biology of Plants, Estación Experimental del Zaidín, Spanish Council of Scientific Research (CSIC), Profesor Albareda 1, 18008 Granada, Spain

in plants metabolism in response to pathogens. This early detection would allow appropriate measures at the right time, and can be used in the field, on the bench (microscopic or leaf level), as well as on canopy through remote sensing and in high-throughput plant phenotyping platforms [1, 2, 6, 7].

Available serological and PCR-based methods to confirm disease diagnosis, as well as visual rating procedures, are just some of the conventional methods for pathogen detection. These more common methods are effective, although they are labor-intensive, time-consuming and often result in delayed diagnosis. In contrast, novel analysis based on imaging sensors can effectively detect early infections directly in the field [8, 9]. In this context, imaging techniques are powerful non-destructive tools for precision agriculture, providing crucial information for decision-making and for determining the right timing for procedures to be applied [10]. These achievements are related both to the development of non-invasive, high-resolution optical sensors and of data analysis methods to deal with the large amount of data generated due to the high resolution, size and complexity rendered by these sensors [9]. Highly sophisticated and innovative methods of data analysis for complex plant-pathogen systems facilitate disease detection and expand the visual and/or molecular approaches for plant disease assessment [11].

2 Imaging kinetics of chlorophyll fluorescence

Kautsky and Hirsch [12] first described changes in red fluorescence (F680) after illumination of dark-adapted plants with photosynthetically active light. In simple words, this effect is due to the competition between photosystem II (PSII) photochemistry and processes of energy dissipation (as heat and fluorescence in the red region of the spectrum) for excitation energy in the pigment antenna of PSII. Therefore, the study of red chlorophyll fluorescence (Chl-F) kinetics provides information on the efficiency of PSII and indirectly on the CO_2 assimilation rate [13]. It has been used for decades as an excellent technique for research on the light-dependent phase of photosynthesis. A great number of Chl-F parameters associated with photosynthetic activity are obtained by Chl-F induction kinetics and subsequent quenching analysis. Some coefficients are related to (i) photochemical processes, like F_V/F_M, the maximum quantum efficiency of PSII (F_V/F_M), and Φ_{PSII}, which represents the effective quantum yield of PSII [14]; (ii) non-photochemical processes related to energy dissipation, estimated by non-photochemical quenching (NPQ) [15]. Also, the red chlorophyll fluorescence decrease ratio (RFd) is directly correlated to the net photosynthetic rates of leaves [16, 17]. Many other Chl-F parameters related to photosynthesis have been reviewed by several authors, e.g. [18–20]. Images of such Chl-F parameters could be good stress indicators to monitor pathogenesis [1]. A recent review by Murchie and Lawson [21] addresses important questions on how to measure Chl-F kinetics, paying special attention to field measurements and their application in plant phenotyping and remote sensing of crop management.

Imaging kinetics of chlorophyll fluorescence imaging (Chl-FI) is a useful tool to study the spatial and temporal heterogeneity of leaf photosynthesis under biotic stress. Thus, Chl-FI adds spatial resolution to the information obtained by conventional fluorometers. Changes in Chl-FI parameters could be related to physiological alterations in plants infected by viruses [4, 5, 22–28], bacteria [29–34] and fungi [35–38].

2.1 Chlorophyll fluorescence imaging to monitor plants infected with viruses

Work on the early responses of chloroplasts to viral infection demonstrate photoinhibitory damage in the infected plants [22–25, 39]. Chl-FI measurements have been carried out in both inoculated and systemically-infected leaves during viral challenge, showing photosynthesis impairment in symptomatic and asymptomatic areas during pathogenesis [4, 5, 24, 25, 27]. In some cases, the rate of photosynthetic inhibition is associated to the severity of the symptoms; however, changes in some fluorescence parameters could precede the development of symptoms, allowing a presymptomatic detection of the disease [40]. Correlation between the pattern of Chl-FI quenching and virus distribution in leaves was found during the infection of pepper mild mottle virus (PMMoV) in *Nicotiana benthamiana* plants [4, 5] as well as in *Abutilon mosaic* virus-infected *Abutilon striatum* leaves [24, 25].

Asymptomatic leaves of *N. benthamiana* infected with PMMoV, showed low NPQ values around the invasion front, suggesting enhancement of the photosynthetic electron transport rate. In the areas already invaded by the pathogen, high NPQ values were detected. Thus, the leaf area showing higher NPQ values increased along the infection time, parallel to the spreading of the virus across the leaf. At the latest stages of infection, the leaves display the lowest NPQ values, denoting a loss in functionality in the chloroplast, presumably related to senescence (Figure 1). Virus-induced changes on the NPQ leaf pattern were visible

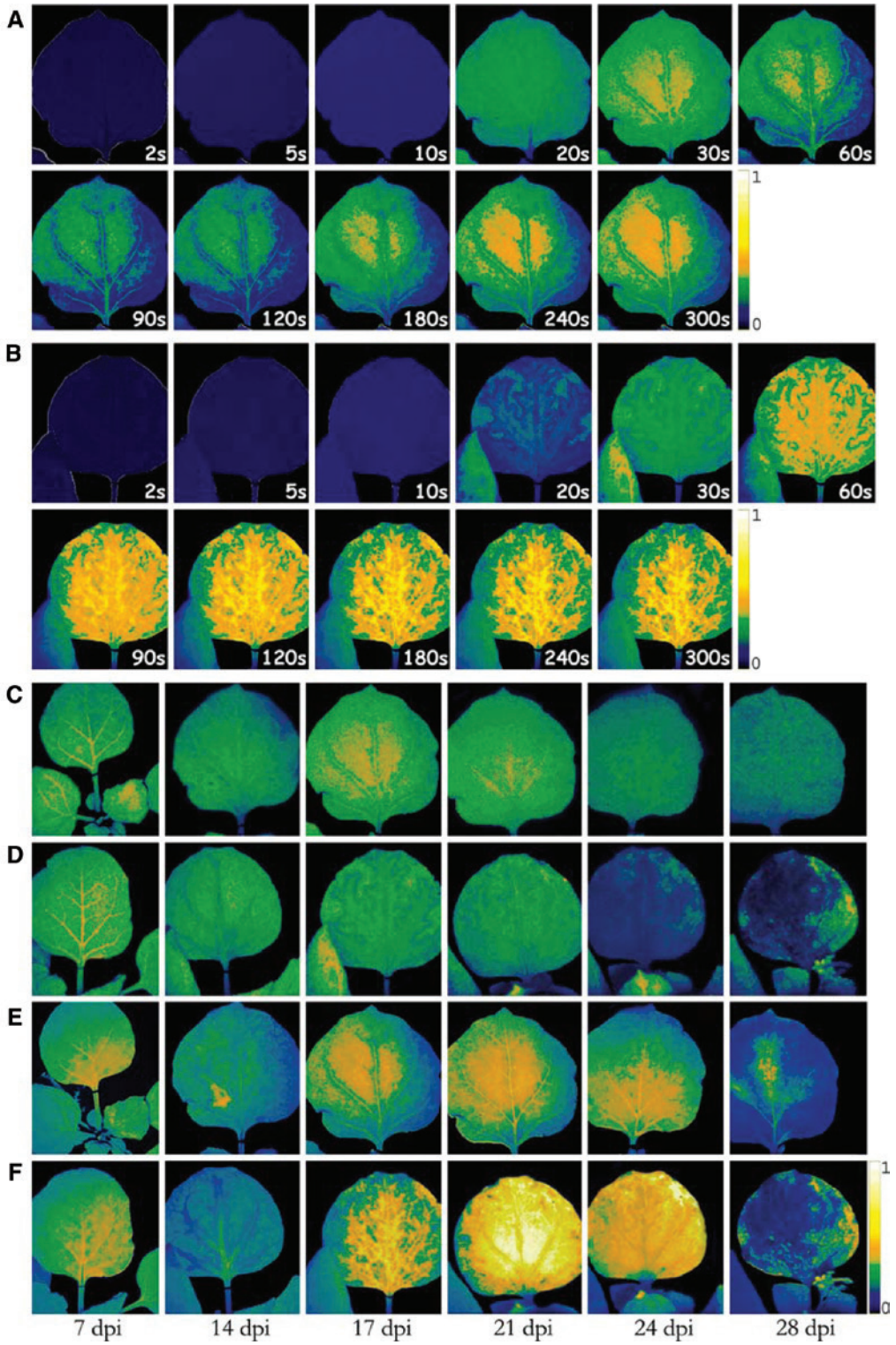

Figure 1: Images of non-photochemical quenching (NPQ) kinetics at 17 dpi of healthy and *Pepper mild mottle virus* Italian strain (PMMoV-I) infected *Nicotiana benthamiana* plants: kinetics during chlorophyll fluorescence induction from healthy (A) and asymptomatic leaves from infected plants (B) at 17 dpi. NPQ after 30 s of Kautsky induction kinetics (NPQ_{30}) images at different dpi from healthy (C) and asymptomatic leaves of infected plants (D). Images of NPQ at steady state (300 s, NPQ_{300}) from healthy (E) and asymptomatic leaves of PMMoV-I infected plants (F) during pathogenesis. The colour scale bar indicates the NPQ intensity of the leaf pixels given in false colors from high (white) to low (blue) values. Figure reproduced from Pérez-Bueno et al. [4] with permission.

before viral elements could be detected by either tissue print or Northern blot. The correlation found between the increase in NPQ and the location of the virus strongly supports the idea that the local rise of NPQ is associated with the presence of the pathogen in the area [4]. The discharge of the virus into the leaf has been proposed to produce an impairment of the photosynthetic electron transport chain (revealed as lower F_V/F_M and Φ_{PSII} values). Then, the excess excitation energy would be dissipated (measured as higher NPQ values) to avoid photoinhibition. This effect takes place progressively in each downstream leaf invaded by the virus. Therefore, Chl-FI proved to be an excellent technique for real-time tracking of pathogen movement in the host plant, providing valuable images about the movement of the virus through the vascular system and its subsequent unloading from the phloem into the mesophyll and spreading across the leaves [5].

Chl-FI was combined with metabolic profiling to study alterations in the primary metabolism of grapevine (*Vitis vinifera* 'Malvasia de Banyalbufar') upon infection with *Grapevine leafroll associated virus 3* (GLRaV-3). The F_V/F_M, Φ_{PSII} and NPQ parameters showed photoinhibition of PSII in infected plants, suggesting a loss of functionality in the chloroplast. The decrease in the accumulation of some photorespiratory intermediates found in infected plants correlated with their increase in NPQ [28].

Kyselákova et al. [41] investigated photosynthetic alterations in pea leaves infected systemically by *Pea enation mosaic virus*. Chl-FI revealed a decrease of Φ_{PSII} and associated photoprotective responses, an increase in non-photochemical quenching and accumulation of de-epoxidized xanthophylls.

Spoustova et al. [42] used Chl-FI to study the impact of *Potato virus Y* (PVY) on the photosynthesis of non-transgenic and transgenic Pssu-ipt tobacco plants, overproducing endogenous cytokinins. Among the fluorescence parameters, NPQ proved to be most useful in assessing the differences between healthy transgenic and wild-type plants, as well as in the analysis of PVY infection in tobacco plants, although presymptomatic detection was not possible in this host-pathogen system.

Rys et al. [43] compared a compatible (PMMoV) with an incompatible [*Obuda pepper virus* (ObPV)] pepper-tobamovirus interaction by Chl-FI and other non-invasive techniques. After the appearance of necrotic lesions, due to inoculation with ObPV, strong inhibition of photochemical energy conversion was observed in these areas; however, leaf tissues adjacent to these inactive areas showed elevated Φ_{PSII} and F_V/F_M values. PMMoV led to decreased PSII efficiency, but these responses were much weaker than in the case of infection by ObPV.

Standard Chl-F parameters do not always show clear differences between healthy and infected tissues. However, in some cases, combinatorial imaging methods could be used to map pathogen infection [30, 44]. Combinatorial imaging analysis is an advance statistical approach that renders new parameters with no physiological meaning, but offers the highest contrast between control and infected plants in the early stages of the infection. A similar approach was used by Pineda et al. [27] to follow the infection of two strains of PMMoV on *N. benthamiana*. In this case, combinatorial imaging revealed the infection earlier than any of the individual Chl-F parameters. Moreover, differences in detection time between the two PMMoV-strains correlated with the virulence of the strains. Detection of viral infection using combinatorial imaging preceded viral location in asymptomatic leaves by tissue printing.

2.2 Chlorophyll fluorescence imaging to monitor plants infected with bacteria

Imaging analysis of the changes of photosynthesis parameters during bacterial challenge in both compatible and incompatible interactions has been object of special attention [31, 33, 34, 45, 46]. An avirulent strain of *Pseudomonas syringae* pv. *glycinea* inducing hypersensitive response (HR) on soybean causes a decrease in Φ_{PSII}, together with an increase in NPQ. Conversely, little changes were observed for a virulent strain able to establish a compatible interaction on the same host [45]. In contrast, Bonfig and collaborators [31] reported a decrease on maximum F_V/F_M, Φ_{PSII} and NPQ in Arabidopsis plants infected with either virulent or avirulent *P. syringae* pv. *tomato* (Pto) strains. Meanwhile, combinatorial imaging and statistical analysis on Arabidopsis leaves infected with *P. syringae* can be used for the detection of the infection prior to the appearance of symptoms [30], and also to distinguish leaf tissues in the early or late phase of infection [44]. Rodríguez-Moreno et al. [46] reported differences between compatible and incompatible interactions in the case of asymptomatic leaf tissues of *Phaseolus vulgaris* plants inoculated with either *P. syringae* pv. *phaseolicola* (Pph) or Pto, respectively. A decrease in NPQ, apparent in both infiltrated and non-infiltrated leaf areas, was observed in Pph-infected plants with respect to mock-control and Pto-infected plants. Moreover, the combined analysis of leaf temperature, Chl-F and green fluorescence (F520) emitted by phenolics on such host-pathogen systems described the specific alterations on primary and secondary metabolism, making it possible to discriminate compatible from

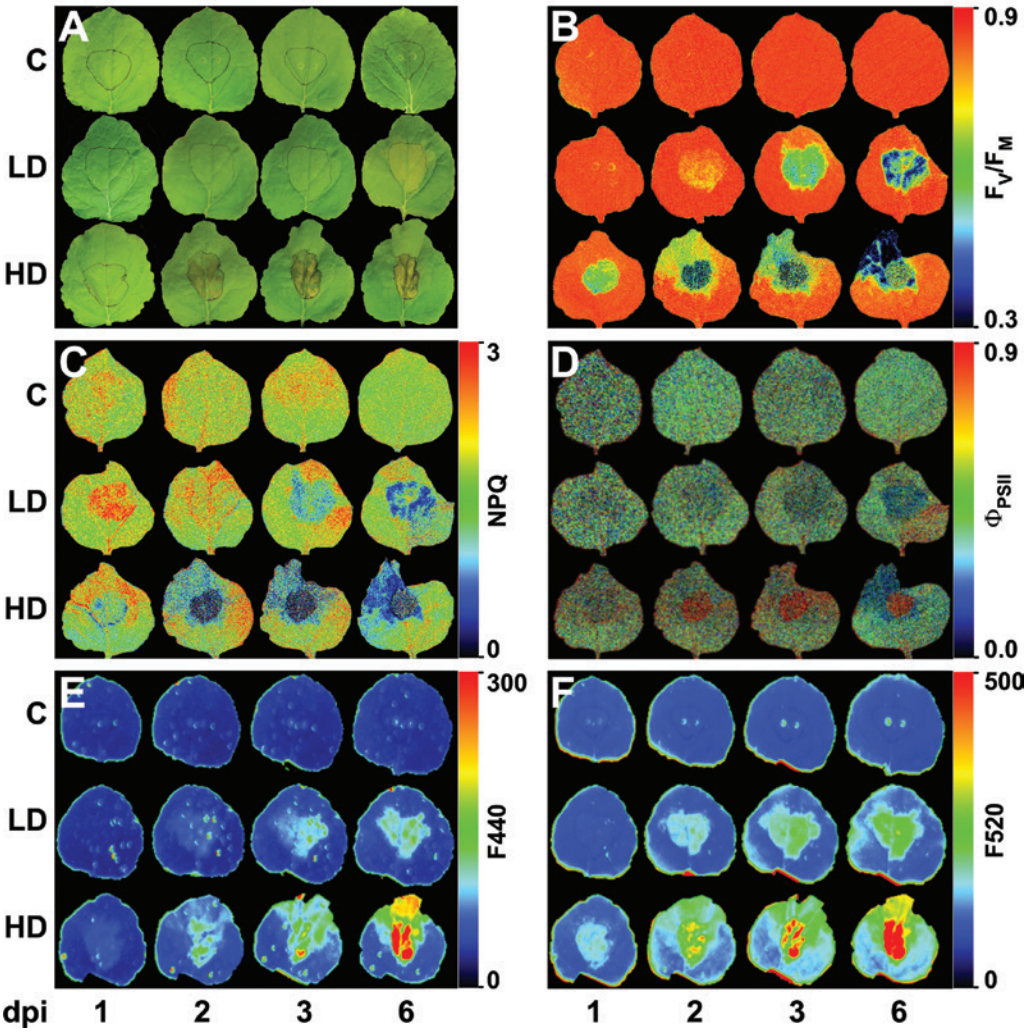

Figure 2: *Nicotiana benthamiana* leaves inoculated with *Dickeya dadantii* at a concentration of 10^4 (LD) or 10^6 (HD) colony forming units per ml or mock-inoculated plants. Evolution of symptoms (A) and images at different post-infection times of: F_V/F_M (maximum quantum efficiency of photosystem II, B), non-photochemical quenching (NPQ) in the light-adapted steady state (C), quantum efficiency of photosystem II in the light-adapted steady state (Φ_{PSII}, D), and fluorescence at 440 nm (E), and 520 nm (F). The infiltrated area was accurately outlined. The false colour-scale used in (B–F) is shown for each parameter. Figure reproduced from Pérez-Bueno et al. [33] with permission.

incompatible *P. syringae-P. vulgaris* interactions early in the presymptomatic phase of the infection process [34].

Pérez-Bueno et al. [33] imaged the host response of tissue invaded by the necrotrophic bacteria *Dickeya dadantii*, a causal agent of soft-rot disease, at low and high dosage of the bacterial inoculum. Inoculation with *D. dadantii* at a high dose (HD) seemed to overcome plant defense capacity, inducing maceration and tissue death, although it remained restricted to the infiltrated area. In contrast, the output of the defense response to low dose (LD) inoculation was the inhibition of tissue maceration and the limitation of bacterial growth. In this study, *D. dadantii* caused a decrease in Φ_{PSII} and an increase in the capacity for energy dissipation or reversible NPQ on tissues in which the defense response was able to prevent tissue from maceration (Figure 2). The down-regulation of photosynthesis was suggested to be part of the plant defense program to limit carbon source availability for pathogens and/or to redirect carbon into secondary metabolism [47]. Meanwhile, Göhre et al. [48] proposed NPQ to be a positive regulator of pathogen-associated molecular patterns (PAMPs) triggered immunity. According to this model, PAMPs perception would cause a reduction of the PSII subunit PsbS, which would be partially responsible for the decrease in the NPQ capacity. This in turn would cause an increase in the production of reactive oxygen species which are known to play a role in the activation of plant defense.

2.3 Chlorophyll fluorescence imaging to monitor plants infected with fungi

Alterations in the photosynthesis of fungi-infected plants mapped by Chl-FI are also spatially and temporally complex. Infected leaves consist of regions of cells directly invaded by the pathogen and regions that are remote from the fungal colony [24, 36, 37, 49]. The fluorescent parameter best suited for either evaluating damage or carrying out presymptomatic diagnosis depends on the type of infection.

Invasion of bean leaves by rust fungi (*Uromyces appendiculatus*) was revealed by changes in the fluorescence induction kinetics [50]. Cedar needles (*Torreya taxifolia*) infected by the fungus *Pestaliopsis* spp. were identified by an empirical estimate of quantum yield [51], which was also used by Bowyer et al. [52] to visualize the impact of fungal phytotoxins in hibiscus leaves (*Hibiscus sabdariffa*). Imaging of Φ_{PSII} was also used to assess the impact of the fungal pathogen *Ascochyta rabiei*, which altered source-sink relationships in chickpea leaves [53]. Soukupová et al. [54] proposed an experimental algorithm to identify the combination of fluorescence parameters providing the highest contrast between affected and unaffected plants in canola (*Brassica napus*) and white mustard (*Sinapis alba*) leaves treated with phytotoxins produced by *Alternaria brassicae*. Changes in the photosynthetic parameters were also visualized during host resistance [38, 55]. A Chl-FI approach of pixel-wise analyses of F_V/F_M was capable of distinguishing resistant and susceptible butterhead and batavia lettuce lines against *Bremia lactucae* [56].

Muniz et al. [57] applied Chl-FI to cashew seedlings inoculated with the fungus *Lasiodiplodia theobromae* to assess any disturbances in the photosynthetic apparatus of the plants before the onset of visual symptoms. Early metabolic perturbations in the chloroplast caused by gummosis could be detected in F_V/F_M images of both whole plants and single leaves. The authors concluded that this parameter could be potentially used in larger-scale screening systems.

Csefalvay et al. [58] assessed the use of Chl-FI in the early stages of *Plasmopara viticola* infection on grapevine, under experimental conditions similar to those occurring in commercial vineyards. F_V/F_M and Φ_{PSII} were identified as the most sensitive reporters of an infection. Heterogeneous distribution of F_V/F_M and Φ_{PSII} in inoculated leaves was associated with the presence of developing mycelium before the appearance of symptoms and the release of spores.

The suitability of Φ_{PSII} and other parameters calculated from the slow induction kinetics of Chl-F for monitoring the progression of a root disease was evaluated in ginseng plants (*Panax quinquefolius* L.) infected with *Pythium irregulare* Buisman. The results were compared to those obtained by the established methods of pathogen detection [59].

One of the most important soil-borne diseases affecting avocado (*Persea americana* Mill.) crops is white root rot, caused by the fungus *Rosellinia necatrix*. Symptoms in the aerial parts of the plants cannot be recognized in early stages of root infection. Granum et al. [35] found that some Chl-FI parameters (F_M/F_0, F'_V/F'_M and F'_V/F'_0) revealed significant differences between healthy and stressed plants at an earlier stage of the infection, suggesting that the photosynthetic apparatus was already affected in the presymptomatic phase. However, F_V/F_M decreased dramatically only when the first symptoms appeared (Figure 3). The decrease in this parameter is indicative of photodamage to PSII, probably due to the water deficit caused by the white root rot.

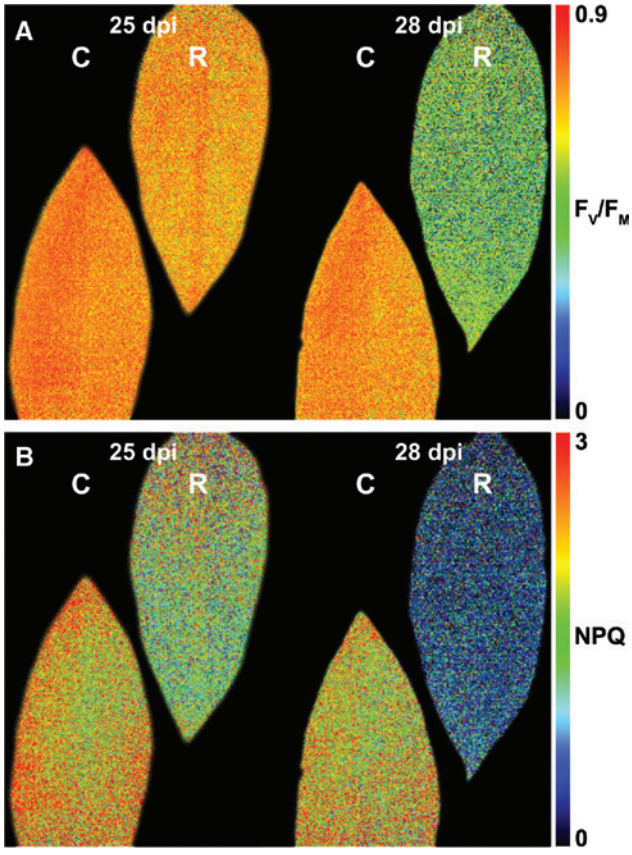

Figure 3: Chlorophyll fluorescence images of maximum quantum efficiency of photosystem II (F_V/F_M) in leaves of a *Rosellinia necatrix*-infected avocado plant (R) and a non-infected control plant (C) at 25 dpi and 28 dpi (A), and average non-photochemical quenching values throughout the infection (B). Figure adapted from Granum et al. [35] with permission.

3 Multicolor fluorescence imaging

The excitation of leaves with long-wavelength UV radiation (320–400 nm) resulted in four characteristic wide fluorescence bands with peaks around 440 nm (blue; F440), 520 nm (green; F520), 690 nm (red; F690) and 740 nm (far-red; F740) [60]. Imaging of fluorescence in those regions of the spectrum after UV excitation [the so-called multispectral or multicolor fluorescence imaging (MCFI)] increases the number of plant processes than can be simultaneously analyzed and provides a promising way to identify specific signatures for a particular stress [61].

The biosynthesis of many phenolic compounds, mainly through the phenylpropanoid pathway, is activated upon stress as part of the plant defense response. Under UV excitation, these compounds can emit blue-green fluorescence (BGF) [62, 63]. The main BGF emitters have been identified for some plant species and have been localized in healthy plants. Such was the case for ferulic acid [64, 65] or chlorogenic acid [66]. More recently, Talamond et al. [67] addressed the location of many phenolics using multiphoton microscopy. In leaves of healthy plants, the strongest BGF corresponds to the epidermis, vascular tissue and also mesophyll cell walls. Meanwhile, F690 and F740 are emitted by chlorophyll *a* [68]. However, red and far-red fluorescence (F740) are not strictly related to photosynthetic activity, since they are triggered by UV light, which is not photosynthetically active. In contrast to BGF, F690 and F740 are mainly emitted by the chloroplasts in the mesophyll and guard cells [62].

The fluorescence ratios F440/F520, F440/F690, F440/F740, and F690/F740 are often used in plant stress studies: F440/F690 and F440/F740 are frequently good as very early stress indicators, whereas F440/F520 reveals changes in plant metabolism after long stress exposure. Meanwhile, the F690/F740 ratio is inversely proportional to the chlorophyll content of a tissue [60, 63, 69].

3.1 MCFI to monitor plants infected with virus

MCFI has proved to be very useful in many experimental plant-virus systems. Pineda et al. [70] monitored a systemic viral infection in PMMoV-infected *N. benthamiana* and detected alterations in both red and BGF emission patterns in response to pathogenesis. It is worth noting here that *N. benthamiana* accumulates high levels of chlorogenic acid bound to the cell walls in response to viral infection [70]. Chinese cabbage infected with *Turnip yellow mosaic virus* showed an increase in the fluorescence ratios F440/F690, F440/F740, and F690/F740 [71]. For this system, the authors concluded that the increase in the intensity of F440 and F520 correlated with higher concentrations of phenylpropanoids in infected plants. Also, tobacco plants challenged with tobacco mosaic virus (TMV), triggering HR, showed an increase in BGF that was related to an increase in the accumulation of scopoletin [72]. During the infection of grapevine with GLRaV-3, the combination of NPQ images with those obtained by MCFI parameters could constitute disease signatures allowing the discrimination between GLRaV-3 infected and non-infected plants at a very early stage of infection, prior to the development of symptoms [28]. Meanwhile, the concentration of flavonols (represented by myricetin, kaempferol and quercetin derivatives) and hydroxycinnamic acids (which include derivatives of caffeic acid) increased following infection by the virus. These compounds could be responsible for the increase in multicolor fluorescence F440, F520 in the leaves, and for changes in the fluorescence ratios F440/F680, F440/F740, F520/F680 and F520/F740, but have little effect on the Chl-F ratio F680/F740.

3.2 MCFI to monitor plants infected with bacteria

Nicotiana benthamiana plants can be infected by *D. dadantii*, a necrotrophic bacterium producing soft rot in a wide range of hosts. Inoculated plants showed higher F440 and F520 than control plants in the early infection process, although F520 was more sensitive than F440 and could indicate infection at an earlier time (Figure 2). The localization of F440 and F520 emitters, first in the apoplast and later inside the vacuoles of mesophyll cells, pointed to an increase in the accumulation of soluble phenolic compounds, rather than bound to the cell walls. Moreover, ferulic acid and scopoletin, two well-known phytoalexins, were found to be increased in bacterial-challenged plants [33].

MCFI was used to test the response of tomato plants to Pto mutants in the multidrug resistance efflux pump MexAB-OprM. Images of F440 and F440/F690 could be used to classify them in terms of virulence [73].

Fluorescence signals were significantly higher in powdery mildew infected sugar beet (*Beta vulgaris* L.) plants compared to the controls, particularly F440, leading to higher F440/F690 in those plants [74]. The authors concluded that fluorescence indices might be used as single or combined indices of successful stress sensing.

3.3 MCFI to monitor plants infected with fungi

Effects of fungal root infection on host secondary metabolism were investigated using *R. necatrix*-infected avocado plants as a model [35]. F440 and F520 increased significantly in the leaves of infected plants, but were only observed at the late-symptomatic stage (32–36 dpi), which is probably caused by an alteration in the optical properties of the leaves due to loss of water from the leaves.

Meanwhile, Konanz et al. [75] used an advanced multicolor imaging system, based on Chl-F and BGF, in combination with an extended data analysis (shape descriptors). The authors found parameters by which they could identify different kinds of fungal symptoms (sugar beet leaf spot, grapevine black rot disease).

4 Thermal imaging

Stomata are pores in the epidermis of leaves. They are formed by two guard cells that determine the aperture of the pore, thereby controlling the gas exchange between the mesophyll of the leaves and the air. While CO_2 necessary for photosynthesis enters the leaf, gaseous water leaves, serving both as driving force for water and nutrient intake in the roots and as cooling system for the leaves. Additionally, stomata are the main natural entry site for pathogens into leaves. Therefore, an accurate control of stomatal closure is essential as part of the plant defense responses triggered by pathogens [76]. Moreover, pathogens often have the ability of manipulating plant signaling pathways, thereby interfering with plant defense. As a result, some pathogens are able to prevent stomatal closure upon detection of pathogens or are even able to reopen them [48, 77–79].

The high resolution of actual thermal cameras allows to picture the behavior of stomata on the plant canopy and even on individual leaves related to biotic stress. Near infrared (NIR) cameras measure leaf and canopy temperature, which inversely correlates with transpiration and stomatal conductance [80–83]. Thermal imaging of plants has been widely used in plant phenotyping mainly to characterize drought susceptibility [84]. Furthermore, thermal imaging combined with Chl-FI has enabled the analysis of spatial and temporal heterogeneity of leaf transpiration and to correlate it with photosynthetic activity. This combination of techniques can reveal presymptomatic responses to pathogens [33, 34, 40].

Thermal imaging has been used to monitor plant stress caused by viruses [3, 85, 86], bacteria [33, 34] and fungi [26, 35, 87].

4.1 Thermal imaging to monitor plants infected with virus

Presymptomatic increases in temperature were visualized on TMV infection sites on tobacco plants, related to HR [85, 88]. Moreover, the same authors compared a viral-induced HR (on a TMV-resistant tobacco line) with an infection by a necrotrophic fungus (*Cercospora* spp. on bean plants), obtaining contradictory effects regarding leaf temperature due to the different ways of infection of both pathogens [26]. In PMMoV-infected *N. benthamiana* plants, thermal imaging showed an increase in the temperature in asymptomatic leaves, before the virus unloaded from the phloem into the tissues [3]. It is concluded that this thermal pattern is due to the systemic invasion of PMMoV.

4.2 Thermal imaging to monitor plants infected with bacteria

Maes et al. [89] described the use of thermography for the detection of bacterial canker [caused by *P. syringae* pv. *actinidiae* (Psa)] in kiwifruit at leaf and orchard scale. At the leaf level, spots of lower temperature appeared shortly after Psa-infection, before any visual symptoms appeared. As the infection developed, spots of higher temperature were observed, partly associated with necrotic tissue. At the orchard level, authors could map the field based on canopy temperature, showing that Psa infects the outer canes rather than the central part of the canopy.

A comparative study was conducted on bean plants developing a compatible and incompatible interaction with two pathovars of *P. syringae*, i.e. Pph and Pto, respectively. An increase in temperature was detected at the infection sites during the first 5 h after infiltration. Pph caused an increase in temperature 1 h after the infiltration of bacteria, 1 h earlier than in those plants infiltrated with Pto; this differential behavior could be explained by the absence of a known toxin able to interfere with stomatal regulation in Pph [34].

The establishment of HR could also be monitored by thermal imaging in *Nicotiana sylvestris* plants inoculated with the bacterium *Erwinia amylovora* [88]. The authors linked the observed low temperature (which preceded the necrosis by several hours) with mitochondrial activity, since mutants in this organelle did not show such high transpiration rate. They proposed that mitochondria are the major source of energy required for stomatal activity, or alternatively, non-phosphorylating respiratory enzymes from this organelle could compensate for a slight temperature decrease by heat dissipation.

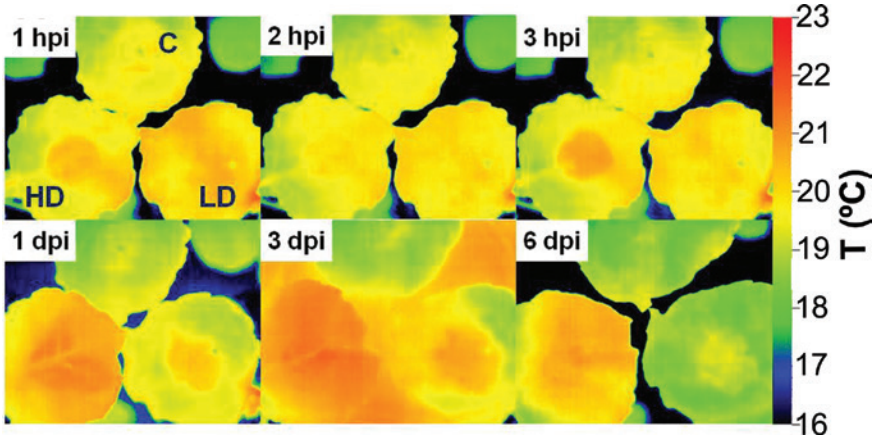

Figure 4: Infrared emission of *Nicotiana benthamiana* leaves inoculated with *Dickeya dadantii* at 10^4 (LD) or 10^6 (HD) colony forming units per ml, and mock-control, monitored by a thermal camera. False colour-scale thermal images of inoculated and control leaves during the first 6 days post infection. Figure adapted from Pérez-Bueno et al. [33] with permission.

The effect of bacterial infection on stomatal regulation was also analyzed in the experimental system *N. benthamiana – D. dadantii* [33]. During the first hour of post-infiltration the temperature increased rapidly in infiltrated areas, probably as a response to wounding, followed by a second increase in temperature, this time dose-dependent (Figure 4). In this case, the stomatal closure would be triggered by PAMPs perception and controlled by abscisic and salicylic acid, the levels of which were found to be increased.

4.3 Thermal imaging to monitor plants infected with fungi

Thermal imaging has been used in the analysis of many fungal infections attacking aerial parts of the plants. Downy mildew of cucumber, caused by *Pseudoperonospora cubensis*, has been reported to trigger changes in metabolic processes, including the transpiration rate, which could be visualized at an early stage by thermal imaging [90, 91].

Thermal imaging of leaves can also be an appropriate tool to detect soil-borne pathogens, as was the case with *Fusarium* wilt on cucumber plants, in which damage to leaf cells could be detected prior to the development of visible symptoms [92]. On the contrary, the presence of the white root rot – caused by *R. necatrix* – in avocado trees could not be detected presymptomatically by this technique [35]. This could be due to the characteristics of the different host-pathogen interactions.

In the literature, there are many examples of fungal infections on trees studied by thermal imaging. In a study on apple scab, thermal imaging was proven useful for describing the severity of the disease resulting from the disease stage, resistance of host tissue and differences in the virulence of *Venturia inaequalis* isolates infecting apple trees [93]. The infection by *Phyllosticta* of two conifer species induced a temperature rise in areas surrounding the inoculation site, suggesting a strong activation of stomata closure that would in turn be associated with the inhibition of Φ_{PSII} and the increase in NPQ capacity [87].

Several authors have successfully addressed the application of thermal imaging to the detection of fungal diseases in crop fields. Stoll et al. [94] analyzed the infection caused by *P. viticola* in grapevine at different levels of the water status. The analysis of thermal images showed that pathogen development caused an increase in leaf temperature at the point of infection in irrigated vines. In contrast, the plants under severe water stress (non-irrigated) showed a lower temperature at the sites of inoculation. A recent study by Calderón et al. [95] describes an automatic procedure for the early detection of *Verticillium* wilt (VW) infection in olive trees to design focalized control strategies at a large scale. Considering that VW is related to physiological alterations shown by spectral changes, the procedure combined various vegetation indices obtained from thermal and high-resolution hyperspectral imagery. Indeed, thermal imaging appears a useful technique when combined with other imaging techniques. Oilseed rape (*Brassica napus* L.) is host for several species belonging to the genus *Alternaria*. Among all the imaging techniques employed in this study, the results obtained by thermography revealed significant changes in infected leaves. Differences in temperature, which depended on the *Alternaria*

species, were observed in various stages of the infection [96]. Hellebrand et al. [97] studied the possibility of detecting wheat plants infected by powdery mildew (*Blumeria graminis*) using thermal and NIR imaging under laboratory and field conditions. The authors concluded that NIR imaging was not suitable for identification of infested plants while thermal imaging was useful under laboratory conditions.

5 Future prospects for imaging sensors in plant phenotyping and remote sensing

Besides possible alterations in leaf structure and morphology, plant pathogens usually affect plant transpiration rates, primary and secondary metabolism and interaction with sunlight. Sensors measuring fluorescence, temperature or even reflectance can be useful tools for the identification, detection and quantification of plant diseases. Using several imaging techniques in parallel could allow disease detection in the absence of visible symptoms and therefore the early identification of emerging diseases in crops [9].

Chl-FI has successfully been used in biotic stress detection in the laboratory, as indicated by the vast amount of information on this topic in the literature. Measuring photosynthesis by Chl-F at the canopy level is challenging because the technique implies the use of saturating light pulses. This limitation has been solved by the use of laser beams. Further improvements in the field include laser-induced fluorescence transients and sun-induced fluorescence (passive estimation of Chl-F from solar reflectance spectra) [7, 11, 98].

Thermal sensors detect early changes in transpiration due to both air- and soil-borne pathogens. However, thermography in crop fields is strongly affected by the microclimate of the plants. The data generated by thermal sensors require background soil corrections and reference temperatures of non-transpiring and/or fully transpiring neighbor canopies ([99] and references therein). The impact of environmental conditions, such as wind and transient cloudiness, has also to be taken into account to interpret plant temperature correctly.

Precision agriculture can make use of in-field imaging technologies to evaluate disease severity, as well as the incidence and progression of the disease. Based on this information, guidance is provided for decisions to further organize or direct protective activities in crop fields and greenhouses. The optical sensors can also be implemented in plant phenotyping programs designed to characterize the level of susceptibility and/or resistance of different genotypes to particular pathogens and to evaluate some plant defense reactions.

The quality, quantity and complexity of the data that can be obtained from sensors have dramatically increased in the last years, The high spectral, spatial and temporal resolution of these data require the use of advanced mathematical methods of data handling, analysis and interpretation [100–102].

Acknowledgments: This work was supported by a grant from Junta de Andalucía (P12-AGR-0370).

References

1. Barón M, Flexas J, Delucia EH. Photosynthetic responses to biotic stress. In: Flexas J, Loreto F, Medrano H, editors. Cambridge: Cambridge University Press, 2012;1:331–50.
2. Rolfe SA, Scholes JD. Chlorophyll fluorescence imaging of plant-pathogen interactions. Protoplasma 2010;247:163–75.
3. Chaerle L, Pineda M, Romero-Aranda R, Van der Straeten D, Barón M. Robotized thermal and chlorophyll fluorescence imaging of pepper mild mottle virus infection in *Nicotiana benthamiana*. Plant Cell Physiol 2006;47:1323–36.
4. Pérez-Bueno ML, Ciscato M, VandeVen M, García-Luque I, Valcke R, Barón M. Imaging viral infection: studies on *Nicotiana benthamiana* plants infected with the pepper mild mottle tobamovirus. Photosynth. Res 2006;90:111–23.
5. Pineda M, Olejnícková J, Cséfalvay L, Barón M. Tracking viral movement in plants by means of chlorophyll fluorescence imaging. J. Plant Physiol 2011;168:2035–40.
6. Nilson HE. Remote sensing and image analysis in plant pathology. Annu Rev Phytopathol 1995;15:489–527.
7. Fiorani F, Rascher U, Jahnke S, Schurr U. Imaging plants dynamics in heterogenic environments. Curr Opin Biotechnol 2012;23:227–35.
8. Martinelli F, Scalenghe R, Davino S, Panno S, Scuderi G, Ruisi P, et al. Advanced methods of plant disease detection. A review. Agron Sustain Dev 2014;35:1–25.
9. Behmann J, Mahlein A-K, Rumpf T, Römer C, Plümer L. A review of advanced machine learning methods for the detection of biotic stress in precision crop protection. Precis Agric 2015;16:239–60.
10. Usha K, Singh B. Potential applications of remote sensing in horticulture – A review. Sci Hortic 2013;153:71–83.
11. Mahlein A-K. Plant disease detection by imaging sensors – parallels and specific demands for precision agriculture and plant phenotyping. Plant Dis 2016;100:241–51.
12. Kautsky H, Hirsch A. Neue Versuche zur Kohlensäureassimilation. Naturwissenschaften 1931;19:964–4.
13. Baker NR. Chlorophyll fluorescence: a probe of photosynthesis in vivo. Annu Rev Plant Biol 2008;59:89–113.

14. Genty B, Briantais J-M, Baker NR. The relationship between the quantum yield of photosynthetic electron transport and quenching of chlorophyll fluorescence. Biochim Biophys Acta 1989;990:87–92.
15. Bilger W, Björkman O. Role of the xanthophyll cycle in photoprotection elucidated by measurements of light-induced absorbance changes, fluorescence and photosynthesis in leaves of *Hedera canariensis*. Photosynth Res 1990;25:173–85.
16. Lichtenthaler HK, Babani F, Langsdorf G. Chlorophyll fluorescence imaging of photosynthetic activity in sun and shade leaves of trees. Photosynth Res 2007;93:235–44.
17. Lichtenthaler HK, Langsdorf G, Lenk S, Buschmann C. Chlorophyll fluorescence imaging of photosynthetic activity with the flash-lamp fluorescence imaging system. Photosynthetica 2005;43:355–69.
18. Maxwell K, Johnson GN. Chlorophyll fluorescence – a practical guide. J Exp Bot 2000;51:659–68.
19. Roháček K, Barták M. Technique of the modulated chlorophyll fluorescence: basic concepts, useful parameters, and some applications. Photosynthetica 1999;37:339–63.
20. Schreiber U, Schliwa U, Bilger W. Continuous recording of photochemical and non-photochemical chlorophyll fluorescence quenching with a new type of modulation fluorometer. Photosynth Res 1986;10:51–62.
21. Murchie EH, Lawson T. Chlorophyll fluorescence analysis: a guide to good practice and understanding some new applications. J Exp Bot 2013;64:3983–98.
22. Balachandran S, Osmond CB. Susceptibility of tobacco leaves to photoinhibition following infection with two strains of *Tobacco mosaic virus* under different light and nitrogen nutrition regimes. Plant Physiol 1994;104:1051–7.
23. Balachandran S, Osmond CB, Daley PF. Diagnosis of the earliest strain-specific interactions between *Tobacco mosaic virus* and chloroplasts of tobacco leaves in vivo by means of chlorophyll fluorescence imaging. Plant Physiol 1994;104:1059–65.
24. Osmond CB, Daley PF, Badger MR, Lüttge U. Chlorophyll fluorescence quenching during photosynthetic induction in leaves of *Abutilon striatum* Dicks infected with *Abutilon mosaic virus* observed with a field-portable system. Bot Acta 1998;111:390–7.
25. Lohaus G, Heldt HW, Osmond CB. Infection with phloem limited *Abutilon mosaic virus* causes localized carbohydrate accumulation in leaves of *Abutilon striatum*: relationships to symtom development and effects on chlorophyll fluorescence quenching during photosynthetic induction. Plant Biol 2000;2:161–7.
26. Chaerle L, Hagenbeek D, De Bruyne E, Valcke R, Van der Straeten D. Thermal and chlorophyll-fluorescence imaging distinguish plant-pathogen interactions at an early stage. Plant Cell Physiol 2004;45:887–96.
27. Pineda M, Soukupova J, Matous K, Nedbal L, Baron M. Conventional and combinatorial chlorophyll fluorescence imaging of tobamovirus-infected plants. Photosynthetica 2008;46:441–51.
28. Montero R, Perez-Bueno ML, Baron M, Florez-Sarasa I, Tohge T, Fernie AR, et al. Alterations in primary and secondary metabolism in *Vitis vinifera* 'Malvasia de Banyalbufar' upon infection with *Grapevine leafroll associated virus 3* (GLRaV-3). Physiol Plant 2016;157:442–52.
29. Berger S, Papadopoulos M, Schreiber U, Kaiser W, Roits T. Complex regulation of gene expression, photosynthesis and sugar levels by pathogen infection in tomato. Physiol. Plant 2004;122: 419–28.
30. Berger S, Benediktyová Z, Matouš K, Bonfig K, Mueller MJ, Nedbal L, et al. Visualization of dynamics of plant–pathogen interaction by novel combination of chlorophyll fluorescence imaging and statistical analysis: differential effects of virulent and avirulent strains of *P. syringae* and of oxylipins on *A. thaliana*. J Exp Bot 2007;58:797–806.
31. Bonfig KB, Schreiber U, Gabler A, Roitsch T, Berger S. Infection with virulent and avirulent *P. syringae* strains differentially affects photosynthesis and sink metabolism in *Arabidopsis* leaves. Planta 2006;225:1–12.
32. Rodríguez-Moreno L, Pineda M, Soukupová J, Macho AP, Beuzón CR, Nedbal L, et al. Chlorophyll fluorescence imaging for detection of bean response to *Pseudomonas syringae* in asymptomatic leaf areas. In: Fatmi MB, Collmer A, Iacobellis NS, Mansfield JW, Murillo J, Schaad NW, et al. editors. *Pseudomonas syringae* pathovars and related pathogens – identification, epidemiology and genomics. Netherlands: Springer, 2008:37–44.
33. Pérez-Bueno ML, Granum E, Pineda M, Flors V, Rodríguez-Palenzuela P, López-Solanilla E, et al. Temporal and spatial resolution of activated plant defense responses in leaves of *Nicotiana benthamiana* infected with *Dickeya dadantii*. Front Plant Sci 2016;6:1209.
34. Pérez-Bueno ML, Pineda M, Díaz-Casado ME, Barón M. Spatial and temporal dynamics of primary and secondary metabolism in *Phaseolus vulgaris* challenged by *Pseudomonas syringae*. Physiol Plant 2015;153:161–74.
35. Granum E, Pérez-Bueno ML, Calderón CE, Ramos C, de Vicente A, Cazorla FM, et al. Metabolic responses of avocado plants to stress induced by *Rosellinia necatrix* analysed by fluorescence and thermal imaging. Eur J Plant Pathol 2015;142:625–32.
36. Scholes JD, Rolfe SA. Photosynthesis in localised regions of oat leaves infected with crown rust (*Puccinia coronata*): quantitative imaging of chlorophyll fluorescence. Planta 1996;199:573–82.
37. Chou HM, Bundock N, Rolfe SA, Scholes JD. Infection of *Arabidopsis thaliana* leaves with *Albugo candida* (white blister rust) causes a reprogramming of host metabolism. Mol Plant Pathol 2000;2:99–113.
38. Swarbrick PJ, Schulze-Lefert P, Scholes JD. Metabolic consequences of susceptibility and resistance (race-specific and broad-spectrum) in barley leaves challenged with powdery mildew. Plant Cell Environ 2006;29:1061–76.
39. Balachandran S, Hull RJ, Martins RA, Vaadia Y, Lucas WJ. Influence of environmental stress on biomass partitioning in transgenic tobacco plants expressing the movement protein of tobacco mosaic virus. Plant Physiol 1997;114:475–81.
40. Chaerle L, Leinonen I, Jones HG, Van der Straeten D. Monitoring and screening plant populations with combined thermal and chlorophyll fluorescence imaging. J Exp Bot 2007;58:773–84.
41. Kyseláková H, Prokopová J, Nauš J, Novák O, Navrátil M, Šafářová D, et al. Photosynthetic alterations of pea leaves infected systemically by *Pea enation mosaic virus*: A coordinated decrease in efficiencies of CO_2 assimilation and photosystem II photochemistry. Plant Physiol Biochem 2011;49:1279–89.
42. Spoustova P, Synkova H, Valcke R, Cerovska N. Chlorophyll a fluorescence as a tool for a study of the *Potato virus Y* effects on photosynthesis of nontransgenic and transgenic Pssu-ipt tobacco. Photosynthetica 2013;51:191–201.
43. Rys M, Juhász C, Surówka E, Janeczko A, Saja D, Tóbiás I, et al. Comparison of a compatible and an incompatible pepper-tobamovirus interaction by biochemical and non-

invasive techniques: Chlorophyll a fluorescence, isothermal calorimetry and FT-Raman spectroscopy. Plant Physiol Biochem 2014;83:267–78.
44. Matouš K, Benediktyova Z, Berger S, Roitsch T, Nedbal L. Case study of combinatorial imaging: what protocol and what chlorophyll fluorescence image to use when visualizing infection of *Arabidopsis thaliana* by *Pseudomonas syringae*? Photosynth Res 2006;90:243–53.
45. Zou J, Rodriguez-Zas S, Aldea M, Li M, Zhu J, Gonzalez DO, et al. Expression profiling soybean response to *Pseudomonas syringae* reveals new defense-related genes and rapid HR-specific downregulation of photosynthesis. Mol Plant Microbe Interact 2005;18:1161–74.
46. Rodríguez-Moreno L, Pineda M, Soukupová J, Macho AP, Beuzón CR, Barón M, et al. Early detection of bean infection by *Pseudomonas syringae* in asymptomatic leaf areas using chlorophyll fluorescence imaging. Photosynth Res 2008;96:27–35.
47. Bolton MD. Primary metabolism and plant defense – fuel for the fire. Mol Plant Microbe Interact 2009;22:487–97.
48. Göhre V, Jones AM, Sklenář J, Robatzek S, Weber AP. Molecular crosstalk between PAMP-triggered immunity and photosynthesis. Mol Plant Microbe In 2012;25:1083–92.
49. Meyer S, Saccardt AK, Rizza F, Genty B. Inhibition of photosynthesis by *Colletotrichum lindemuthianum* in bean determined by chlorophyll fluorescence imaging. Plant Cell Environ 2001;24:947–55.
50. Peterson RB, Aylor DE. Chlorophyll fluorescence induction in leaves of *Phaseolus vulgaris* infected with bean rust (*Uromyces appendiculatus*). Plant Physiol 1995;108:163–71.
51. Ning L, Edwards GE, Strobel GA, Daley LS, Callis JB. Imaging fluorometer to detect pathological and physiological change in plants. Appl Spectrosc 1995;49:1381–9.
52. Bowyer WJ, Ning L, Daley LS, Strobel GA, Edwards GE, Callis JB. In vivo fluorescence imaging for detection of damage to leaves by fungal phytotoxins. Spectroscopy 1998;13:36–44.
53. Esfeld P, Siebke K, Weis E. Local defence-related shift in the carbon metabolism in chickpea leaves induced by a fungal pathogen. In: Mathis P, editor. Photosynthesis from light to biosphere, Vol. 5. Dordrecht: Kluwer Academic Publishers, 1995;663–6.
54. Soukupová J, Smatanová S, Nedbal L, Jegorov A. Plant response to destruxins visualized by imaging of chlorophyll fluorescence. Physiol Plant 2003;118:399–405.
55. Repka V. Chlorophyll-deficient mutant in oak (*Quercus petraea* L.) displays an accelerated hypersensitive-like cell death and an enhanced resistance to powdery mildew disease. Photosynthetica 2002;40:183–93.
56. Bauriegel E, Brabandt H, Gärber U, Herppich WB. Chlorophyll fluorescence imaging to facilitate breeding of *Bremia lactucae*-resistant lettuce cultivars. Comput Electron Agric 2014;105:74–82.
57. Muniz CR, Freire FC, Viana FM, Cardoso JE, Sousa CA, Guedes MI, et al. Monitoring cashew seedlings during interactions with the fungus *Lasiodiplodia theobromae* using chlorophyll fluorescence imaging. Photosynthetica 2014;52:529–37.
58. Csefalvay L, Di Gaspero G, Matous K, Bellin D, Ruperti B, Olejnickova J. Pre-symptomatic detection of *Plasmopara viticola* infection in grapevine leaves using chlorophyll fluorescence imaging. Eur J Plant Pathol 2009;125:291–302.
59. Ivanov DA, Bernards MA. Chlorophyll fluorescence imaging as a tool to monitor the progress of a root pathogen in a perennial plant. Planta 2016;243:263–79.
60. Buschmann C, Lichtenthaler HK. Principles and characteristics of multi-colour fluorescence imaging of plants. J Plant Physiol 1998;152:297–314.
61. Lenk S, Chaerle L, Pfundel EE, Langsdorf G, Hagenbeek D, Lichtenthaler HK, et al. Multispectral fluorescence and reflectance imaging at the leaf level and its possible applications. J Exp Bot 2007;58:8.
62. Lichtenthaler HK, Miehe JA. Fluorescence imaging as a diagnostic tool for plant stress. Trends Plant Sci 1997;2:316–20.
63. Cerovic ZG, Samson G, Morales F, Tremblay N, Moya I. Ultraviolet-induced fluorescence for plant monitoring: present state and prospects. Agronomie 1999;19:543–78.
64. Morales F, Cerovic ZG, Moya I. Time-resolved blue-green fluorescence of sugar beet (*Beta vulgaris* L) leaves. Spectroscopic evidence for the presence of ferulic acid as the main fluorophore of the epidermis. Biochim Biophys Acta 1996;1273:251–62.
65. Lichtenthaler HK, Schweiger J. Cell wall bound ferulic acid, the major substance of the blue-green fluorescence emission of plants. J Plant Physiol 1998;152:272–82.
66. Morales F, Cartelat A, Alvarez-Fernandez A, Moya I, Cerovic ZG. Time-resolved spectral studies of blue-green fluorescence of artichoke (*Cynara cardunculus* L. var. *Scolymus*) leaves: Identification of chlorogenic acid as one of the major fluorophores and age-mediated changes. J Agric Food Chem 2005;53:9668–78.
67. Talamond P, Verdeil J-L, Conéjéro G. Secondary metabolite localization by autofluorescence in living plant cells. Molecules 2015;20:5024–37.
68. Gitelson AA, Buschmann C, Lichtenthaler HK. Leaf chlorophyll fluorescence corrected for re-absorption by means of absorption and reflectance measurements. J Plant Physiol 1998;152:283–96.
69. Buschmann C, Langsdorf G, Lichtenthaler HK. Imaging of the blue, green, and red fluorescence emission of plants: An overview. Photosynthetica 2000;38:483–91.
70. Pineda M, Gaspar L, Morales F, Szigeti Z, Barón M. Multicolor fluorescence imaging of leaves-a useful tool for visualizing systemic viral infections in plants. Photochem Photobiol 2008;84:1048–60.
71. Szigeti Z, Almási A, Sárvári. Changes in the photosynthetic functions in leaves of Chinese cabagge infected with *Turnip yellow mosaic virus*. Acta Biologica Szegediensis 2002;46:137–8.
72. Chaerle L, Lenk S, Hagenbeek D, Buschmann C, Van Der Straeten D. Multicolor fluorescence imaging for early detection of the hypersensitive reaction to *Tobacco mosaic virus*. J Plant Physiol 2007;164:253–62.
73. Vargas P, Farias GA, Nogales J, Prada H, Carvajal V, Baron M, et al. Plant flavonoids target *Pseudomonas syringae* pv. tomato DC3000 flagella and type III secretion system. Environ Microbiol Rep 2013;5:841–50.
74. Leufen G, Noga G, Hunsche M. Fluorescence indices for the proximal sensing of powdery mildew, nitrogen supply and water deficit in sugar beet leaves. Agriculture 2014;4:58–78.
75. Konanz S, Kocsányi L, Buschmann C. Advanced multi-color fluorescence imaging system for detection of biotic and abiotic stresses in leaves. Agriculture 2014;4:79–95.
76. Sawinski K, Mersmann S, Robatzek S, Bohmer M. Guarding the green: pathways to stomatal immunity. Mol Plant Microbe Interact 2013;26:626–32.

77. Zeng W, Melotto M, He SY. Plant stomata: a checkpoint of host immunity and pathogen virulence. Curr Opin Biotechnol 2010;21:599–603.
78. Melotto M, Underwood W, He SY. Role of stomata in plant innate immunity and foliar bacterial diseases. Annu Rev Phytopathol 2008;46:101–22.
79. Melotto M, Underwood W, Koczan J, Nomura K, He SY. Plant stomata function in innate immunity against bacterial invasion. Cell 2006;126:969–80.
80. Jones HG. Use of thermography for quantitative studies of spatial and temporal variation of stomatal conductance over leaf surfaces. Plant Cell Environ 1999;22:1043–55.
81. Chaerle L, Van der Straeten D. Imaging techniques and the early detection of plant stress. Trends Plant Sci 2000;5:495–501.
82. Chaerle L, Van der Straeten D. Seeing is believing: imaging techniques to monitor plant health. Biochim Biophys Acta 2001;1519:153–66.
83. Glenn DM. Infrared and chlorophyll fluorescence imaging methods for stress evaluation. HortScience 2012;47:697–8.
84. Li L, Zhang Q, Huang D. A review of imaging techniques for plant phenotyping. Sensors 2014;14:20078–111.
85. Chaerle L, Van Caeneghem W, Messens E, Lambers H, Van Montagu M, Van der Straeten D. Presymptomatic visualization of plant-virus interactions by thermography. Nat Biotechnol 1999;17:813–16.
86. Aldea M, Frank TD, DeLucia EH. A method for quantitative analysis of spatially variable physiological processes across leaf surfaces. Photosynth Res 2006;90:161–72.
87. Aldea M, Hamilton JG, Resti JP, Zangerl AR, Berenbaum MR, Frank TD, et al. Comparison of photosynthetic damage from arthropod herbivory and pathogen infection in understory hardwood saplings. Oecologia 2006;149:221–32.
88. Boccara M, Boue C, Garmier M, De Paepe R, Boccara AC. Infra-red thermography revealed a role for mitochondria in pre-symptomatic cooling during harpin-induced hypersensitive response. Plant J 2001;28:663–70.
89. Maes WH, Minchin PE, Snelgar WP, Steppe K. Early detection of Psa infection in kiwifruit by means of infrared thermography at leaf and orchard scale. Funct Plant Biol 2014;41:1207–20.
90. Lindenthal M, Steiner U, Dehne HW, Oerke EC. Effect of downy mildew development on transpiration of cucumber leaves visualized by digital infrared thermography. Phytopathology 2005;95:233–40.
91. Oerke EC, Steiner U, Dehne HW, Lindenthal M. Thermal imaging of cucumber leaves affected by downy mildew and environmental conditions. J Exp Bot 2006;57:2121–32.
92. Wang M, Ling N, Dong X, Zhu Y, Shen Q, Guo S. Thermographic visualization of leaf response in cucumber plants infected with the soil-borne pathogen *Fusarium oxysporum* f. sp. *cucumerinum*. Plant Physiol Biochem 2012;61:153–61.
93. Oerke EC, Fröhling P, Steiner U. Thermographic assessment of scab disease on apple leaves. Precis Agric 2011;12:699–715.
94. Stoll M, Schultz HR, Berkelmann-Loehnertz B. Exploring the sensitivity of thermal imaging for *Plasmopara viticola* pathogen detection in grapevines under different water status. Funct Plant Biol 2008;35:281–88.
95. Calderón R, Navas-Cortés JA, Zarco-Tejada PJ. Early detection and quantification of *Verticillium* wilt in olive using hyperspectral and thermal imagery over large areas. Remote Sens 2015;7:5584–610.
96. Baranowski P, Jedryczka M, Mazurek W, Babula-Skowronska D, Siedliska A, Kaczmarek J. Hyperspectral and thermal imaging of oilseed rape (*Brassica napus*) response to fungal species of the genus *Alternaria*. PLoS One 2015;10:e0122913.
97. Hellebrand HJ, Herppich WB, Beuche H, Dammer K-H, Linke M, Flath K. Investigations of plant infections by thermal vision and NIR imaging. International Agrophysics 2006;20:1–10.
98. Fiorani F, Schurr U. Future scenarios for plant phenotyping. Annu Rev Plant Biol 2013;64:267–91.
99. Walter A, Liebisch F, Hund A. Plant phenotyping: from bean weighing to image analysis. Plant Methods 2015;11:1–11.
100. Mahlein A-K, Rumpf T, Welke P, Dehne HW, Plümer L, Steiner U, et al. Development of spectral indices for detecting and identifying plant diseases. Remote Sens Environ 2013;128:21–30.
101. Mahlein AK, Oerke EC, Steiner U, Dehne HW. Recent advances in sensing plant diseases for precision crop protection. Eur J Plant Pathol 2012;133:197–209.
102. Behmann J, Steinrucken J, Plumer L. Detection of early plant stress responses in hyperspectral images. ISPRS J Photogramm 2014;93:98–111.

Epilog

GINKGO BILOBA
[MILLENNIAL TREE]

A tree. Good. Yellow
of autumn. It opens up
to the sky brilliantly, eager
for more light. Screams its splendour
into the garden. And natural,
free, it scatters its colour
straight into the blue. It grows
like a flame, blazes, illuminates
its ancient blood. Dominates
all the air branch by branch.

All the air, branch by branch,
aglow with the yellow abundance
of the tree. Shines
that, only blue, lights
with a golden fire: oriflamme.
Not flag. Joyful fountain
of colour: It knocks up
its golden pole towards the sky.
Its eagerness of many centuries
reaches us. Light from the East.

Yellow. The wind does not
imagine yet, the flight
of its leaves, its brightness
already subdued. The gloomy
evening approaches. Not even foretells
its loneliness, that sorrow
of its branches.

It was certitude,
joy – autumn! - . Beacon
of open light.

Helplessness
afterwards. Where is your beauty?

Elena Martin Vivaldi

Source: The Ginkgo Pages http://kwanten.home.xs4all.nl/. The poem of Elena Martin Vivaldi has been translated into English by Eduardo Arancibia Diaz and Cor Kwant.